

COMPARISON OF THE RADIOMETRIC CORRECTION OF LANDSAT-8 IMAGES BASED ON OBJECT SPECTRAL RESPONSE AND A VEGETATION INDEX

Fadila Muchsin^{1*}, Supriatna¹, Adhi Harmoko¹, Indah Prasasti², Mulia Ina Rahayu³, Liana Fibriawati³, Kuncoro Adi Pradhono³

¹Faculty of Mathematics and Natural Science – University of Indonesia

²Remote Sensing Applications Center – LAPAN

³Remote Sensing Technology and Data Center – LAPAN

*e-mail: fadila.muchsin@lapan.go.id/ila_mc@yahoo.com

Received: 28 June 2021; Revised: 9 September 2021; Approved: 3 January 2022

Abstract. Landsat-8 standard level (level 1T) data received by users still in digital form can be used directly for land cover/land use mapping. These data have low radiometric accuracy when used to produce information such as vegetation indices, biomass, and land cover/land use classification. In this study, radiometric/atmospheric correction was conducted using FLAASH, 6S, DOS, TOA+BRDF and TOA method to eliminate atmospheric disturbances and compare the results with field measurements based on object spectral response and NDVI values. The results of the spectral measurements of objects in paddy fields at harvest time in the Cirebon Regency, West Java, Indonesia show that the FLAASH and 6S method have spectral responses that are close to those of objects in the field compared to the DOS, TOA and TOA+BRDF methods. For the NDVI value, the 6S method has the same tendency as the object's NDVI value in the field.

Keywords: *Landsat-8, atmospheric correction, spectral response, NDVI*

1 INTRODUCTION

The Landsat program for monitoring land use and land cover globally began in 1972 with the launch of the Landsat-1 satellite and continued with Landsat-2 to Landsat-8 in 2013 (Markham & Helder, 2012; Roy et al., 2014; Wulder et al., 2016). The Landsat-8 satellite has two sensors, namely a multispectral Operational Land Imager (OLI) and Thermal Infrared Sensor (TIRS). Landsat-8 OLI data have nine spectral bands with a 30 meter spatial resolution, except for the panchromatic channel (15 meters) and the TIRS data, which have two thermal bands with a 100 meter spatial resolution (Roy et al., 2014). Each band can provide information about various phenomena on the surface of the earth. Landsat-8

data have a temporal resolution of 16 days so can be used to monitor land use and land cover changes consistently and sustainably (Gómez, White, & Wulder, 2016; Loveland & Irons, 2016).

Standard level Landsat-8 data (1T) received by users can be used directly for certain applications such as land use/land cover mapping. The data have low radiometric accuracy if used to produce digital information such as vegetation indices, biomass, or classification of land cover (Prieto-amparan, Villarreal-guerrero, & Martinez-salvador, 2018). Therefore, radiometric correction/calibration is needed to eliminate radiometric disturbances that have not been corrected at the 1T data level, such as the effects of solar radiation, object

geometry and atmospheric disturbances. Radiometric correction is necessary for producing high-quality scientific data to produce more accurate information products such as land cover maps (Pons et al., 2014). The results of radiometric/atmospheric correction are called surface reflectance products (Liang, Member, Fang, & Chen, 2001; E. Vermote, Justice, Claverie, & Franch, 2016).

Radiometric correction based on atmospheric correction methods to produce surface reflectance products has been widely applied and developed, starting with the Top of Atmosphere (TOA) reflectance method to improve radiometric interference resulting from differences in the position of the sun in images with different acquisition dates (Chander, Markham, & Helder, 2009; Hermosilla, Wulder, White, Coops, & Hobart, 2017; Sterckx, 2019). It is therefore important for multitemporal analysis: for example, the Dark Object Subtraction method to improve radiometric interference due to scattering of particles in the atmosphere (Jing, Wei, Jianxin, & Xuning, 2014; Moravec, Komárek, Medina, & Molina, 2021; Prieto-amparan et al., 2018; Rumora, Miler, & Medak, 2020); the

TOA+BRDF method to improve radiometric interference due to differences in the position of the sun and the geometry of objects (Kustiyo, 2017); the second simulation of satellite signals in the solar spectrum (6S) (Lee et al., 2020; E. Vermote et al., 2016); and Fast Line-of-sight Atmospheric Analysis of Spectral Hypercubes (FLAASH) (DianWang, Ma, Xue, & Loiselle, 2019; Moravec et al., 2021). These methods improve atmospheric interference in images arising from scattering and uptake of gas particles and atmospheric molecules such as aerosols, water vapour and ozone. Quantitatively, the presence of interference can be established by noting the spectral response of the object being observed (Congalton, 2015). The radiometric correction method has been widely applied to ascertain, for example, an object's spectral response and vegetation index, and to produce land use/land cover information and forest classification. However, no comparison of the atmospheric correction results from these methods has been made, especially the spectral response of the objects and vegetation index on agricultural land in the West Java region.

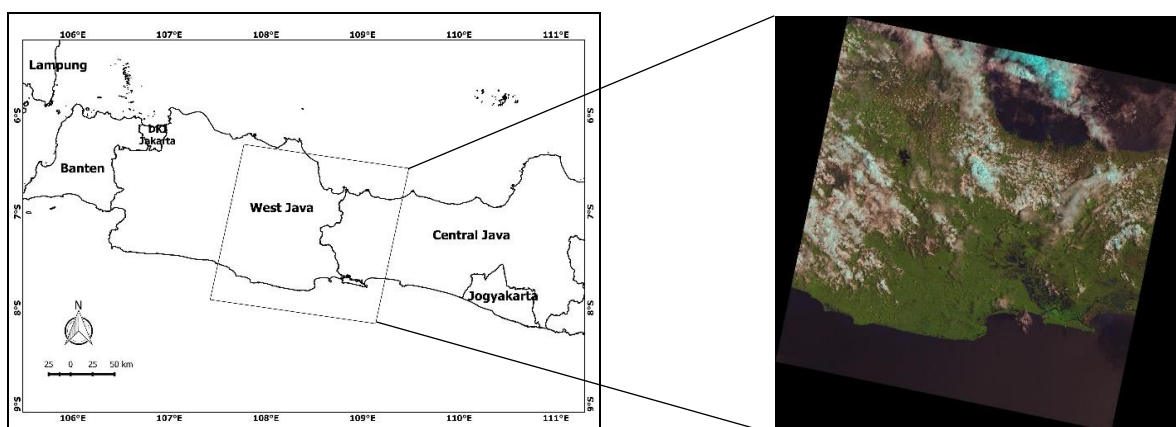


Figure 2-1. Landsat 8 data, Path/Row 121/065, acquisition date October 13th, 2016

The aim of this study therefore is to conduct atmospheric correction of Landsat-8 level-1T data in Cirebon Regency using the above methods and to compare the results with field measurements based on objects' spectral response and vegetation index.

2 MATERIALS AND METHODOLOGY

2.1 Data and Location

The Landsat data used in this study are shown in Figure 2-1. They are Landsat 8 multispectral data (visible and NIR band), Path/Row 121/065, level 1T, 30 m resolution, and cloud cover 34.5 %. The data were acquired from the LAPAN Parepare ground station on October 13th, 2016 at 09.54 WIB (02:54 UTC). The study location were paddy fields in the Cirebon Regency area (coordinates S06030' - S07000' and E108040' - E108048'), in which the object conditions tended to be more homogeneous in order to avoid the reflectance effects of different objects around them (EF Vermote et al., 1997).

Radiometric correction requires information on sensor parameters such as azimuth and elevation angles and radians, which can be obtained from image metadata. The metadata information is shown in Table 2-1.

2.2 Radiometric Correction

Radiometric and atmospheric corrections produce reflectance or surface reflectance and were made using

methods that has been applied to Landsat-8 imageries, namely (1) TOA correction (Chander et al., 2009) (2) Dark Object Substraction (ENVI, 2009; Prieto-amparan et al., 2018); (3) the TOA+BRDF method (Kustiyo, 2017); (4) 6S (E. F. Vermote, Tanré, Deuze, Herman, & Morcrette, 1997; E. Vermote et al., 2016); and (5) FLAASH method (ENVI, 2009).

The 6S and FLAASH correction methods use atmospheric model settings, namely aerosol models for maritime areas with visibility values of 7 km, obtained from visibility measurements of Cakrabhuwana Airport, Cirebon (West Java) on the same date and time as the crossing of the Landsat-8 Satellite. The atmospheric profile model was set for the tropical region, according to the characteristics of Indonesia. The initial visibility value in the FLAASH method was set at 15 km (ENVI, 2009) as image conditions tend to be cloudy.

2.3 Spectral Measurement

Spectral measurement of objects was made using Ocean Optics Spectrometer equipment type: HR4000CG-UV-NIR with a wavelength of visible to NIR of 400 nm - 900 nm. Other equipment used included Garmin Montana 680 GPS to determine the coordinate position of the object being measured.

Table 2-1: Sensor parameter information

| Satellite Image | Azimuth (degree) | Elevation (degree) | Zenith (90 - elevation) (degree) | Band | Q _{cal} _{min} | Q _{cal} _{max} | LMIN _λ | LMAX _λ |
|--|------------------|--------------------|----------------------------------|------|---------------------------------|---------------------------------|-------------------|-------------------|
| Landsat-8 P/R (121/065) October 13th, 2016 | 93.18 | 65.78 | 27.4 | 2 | 1 | 255 | -6.2 | 191.6 |
| | | | | 3 | 1 | 255 | -6.4 | 196.5 |
| | | | | 4 | 1 | 255 | -5 | 152.9 |
| | | | | 5 | 1 | 255 | -5.1 | 241.1 |
| | | | | 6 | 1 | 255 | -1 | 31.06 |
| | | | | 7 | 1 | 255 | -0.35 | 10.8 |

The time measurement was made on the same date and time as the Landsat-8 satellite crossing, namely October 13, 2016 from 09.30 WIB to 12.30 WIB. The location of the measurements was in the paddy fields in the area of Cirebon Regency, covering Suranenggala Sub-district (09.00 - 09.30) WIB, Klangeran (09.30 - 10.00) WIB and Mundu (12.00 - 13.00) WIB (Figure 2-2).

The three locations were chosen because they are close to Cakrabhuwana Airport, meaning the airport's visibility value was still valid. The type of objects measured were watery, vegetative and dry paddy fields in the vegetative, ripening and post-ripening stages, as shown in Table 2-2. However, all the field measurements were not used in the

analysis due to cloud cover problem in the image. Only objects in paddy fields after ripening were analyzed.

2.4 Vegetation Index

The vegetation index that is commonly used to differentiate between the greenness of vegetation based on spectral values is the Normalized Difference Vegetation Index (NDVI) using visible bands, namely the red and near infrared (NIR) bands. NDVI is derived using the formula (Ke, Im, Lee, Gong, & Ryu, 2015):

$$NDVI = (\rho_{nir} - \rho_{red}) / (\rho_{nir} + \rho_{red}) \quad (2-1)$$

where ρ_{red} and ρ_{nir} are reflectance/surface reflectance on the red and NIR bands.

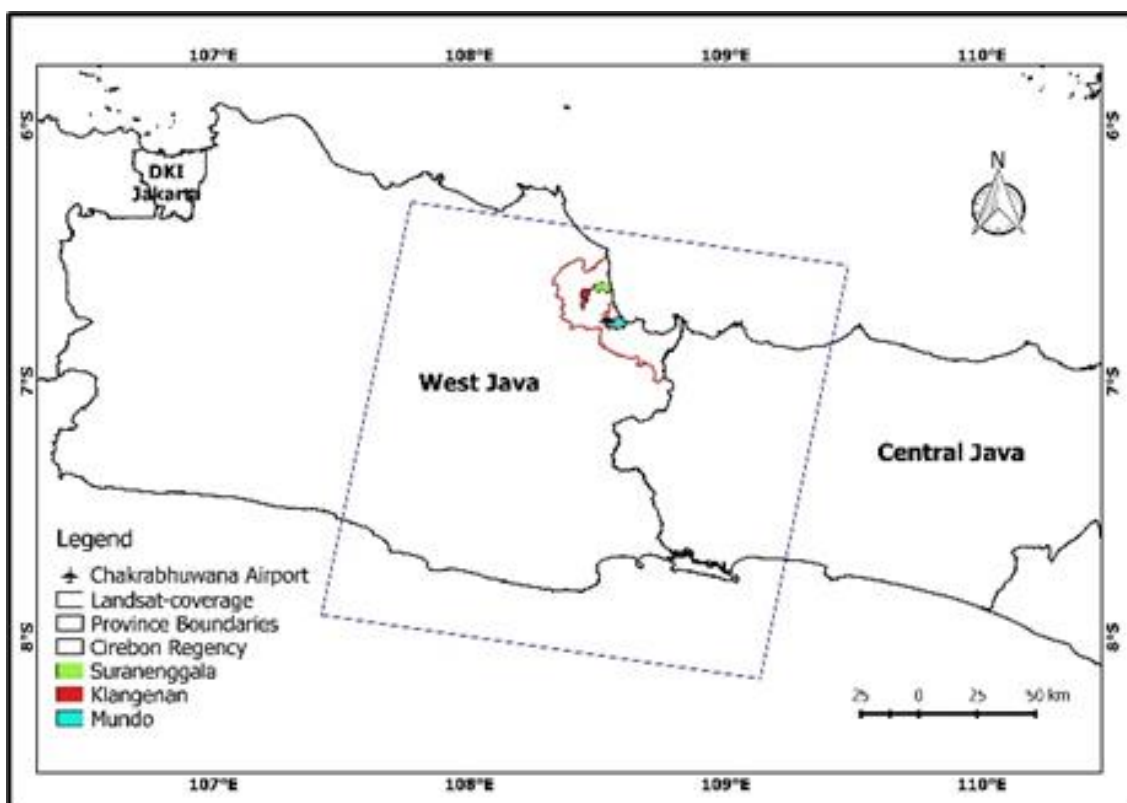











Figure 2-2. Location of the object spectral measurements in the Cirebon regency

Table 2-2: Types of objects measured in the paddy fields, including watery, vegetative and dry paddy fields in Suranenggala, Klangeran and Mundo Sub-districts

| Sub-district | Date / Time | Coordinate | Object phase | Object image |
|--------------|--------------------------------------|-------------------------------|---|---|
| Suranenggala | October 13th, 2016 / 07.42 WIB | S06037'29.5" E108030'16.9" | Ripening phase (generative); watery soil conditions |  |
| | October 13th, 2016 / 08.00 WIB | S06037'29.5" E108029'59.4" | Ripening phase (generative); watery soil conditions |  |
| | October 13th, 2016 / 08.14 WIB | S06037'26.2" E108029'41.0" | Ripening phase (generative); watery soil conditions |  |
| | October 13th, 2016 / 08.14 WIB | S06037'26.1" E108029'19.1" | Ripening phase (generative); watery soil conditions |  |
| Klangeran | October 13th, 2016 / 11.16 WIB | S06039'31.2" E108026'24.8" | Post-ripening phase (stump); slightly dry soil conditions |  |
| | October 13th, 2016 / 11.29 WIB | S06039'24.7" E108026'52.8" | Post-ripening phase (stump); watery soil conditions |  |
| | October 13th, 2016 / 11.47 WIB | S06039'28.3" E108026'28.3" | Vegetative phase; watery soil conditions |  |
| Mundo | October 13th, 2016 / 12.43 WIB | S06046'20.5" E108035'37.6" | Post- ripening phase; unvegetated soil; slightly dry and rather moist conditions |  |
| | October 13th, 2016 / 12.55 WIB | S06046'39.9" E108035'48.2" | Post-ripening phase; a little grass vegetation; slightly watery soil conditions |  |

3 RESULTS AND DISCUSSION

3.1 Object Spectral Responses

Comparison of the object spectral responses with the field measurements could only be made in two locations in the Mundo sub-district, because of cloud cover problems in the image. The object coordinates in location 1 were (S06046'20.5", E108035'37.6") and in location 2 (S06046'39.9", E108035'48.2"). The position of the objects at these locations is shown in Figure 3-1. The time of the measurement at location 1 was 12.43 WIB with cloudy sunny weather conditions and at location 2 it was 12.55, with sunny conditions. Both locations were post-ripening paddy fields, with moist soil conditions and dry vegetation at location 1, and watery soil conditions and low vegetated/grass conditions at location 2. The condition of the two objects in the field are shown in Figure 4.

The spectral response of paddy fields in location 1 has relatively higher reflectance values in the blue band (0.483 μm) and the green band (0.561 μm) for the DOS, TOA and TOA+BRDF,

compared to the results of the field measurements, with the highest being the TOA+BRDF in the blue band and the 6S method in the green band. The FLAASH and 6S values are relatively lower, and closest being the FLAASH method in the blue band and DOS bands in the green band. The spectral response in the red band (0.655 μm) is relatively lower for all the methods and the closest is the TOA+BRDF. In the infrared bands (0.855 μm) tend to be higher for the TOA+BRDF and TOA, lower for the DOS method, and closer to the field measurements for the 6S and FLAASH. The spectral responses of each method are shown in Figure 3-3.

The percentages of the reflectance values for each method compared to the field measurements at location 1 are presented in Table 3-1. They vary for each Band. The highest percentage of field measurements correspond to the TOA and TOA+BRDF because the atmosphere has not been corrected. The FLAASH, 6S and DOS methods tend to be low because in this case atmosphere disturbances have been corrected.

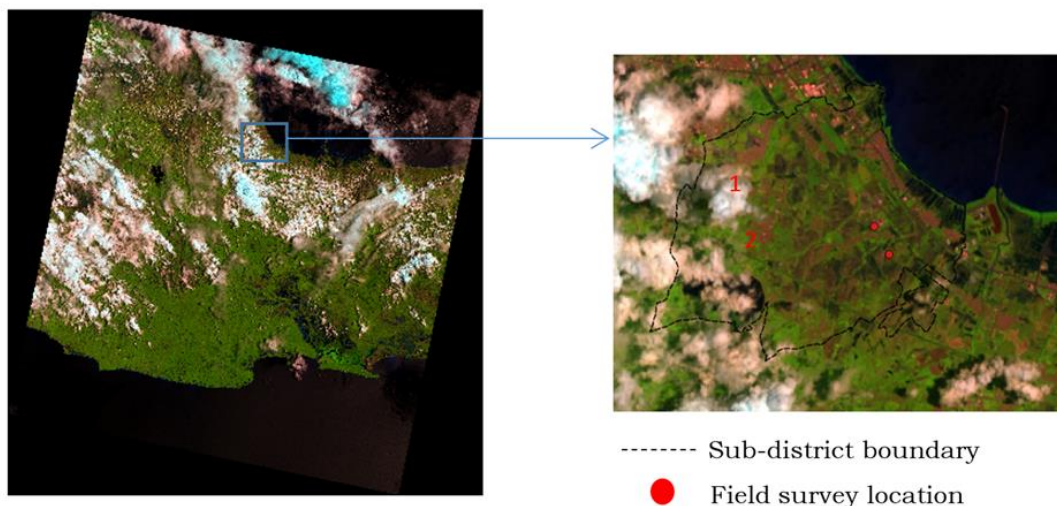


Figure 3-1: Landsat-8 image of object location in Mundo sub-district; acquisition date October 13th 2016, band combination RGB 654



Figure 3-2. (a) Condition of paddy fields at location 1; (b) condition of paddy fields at location 2

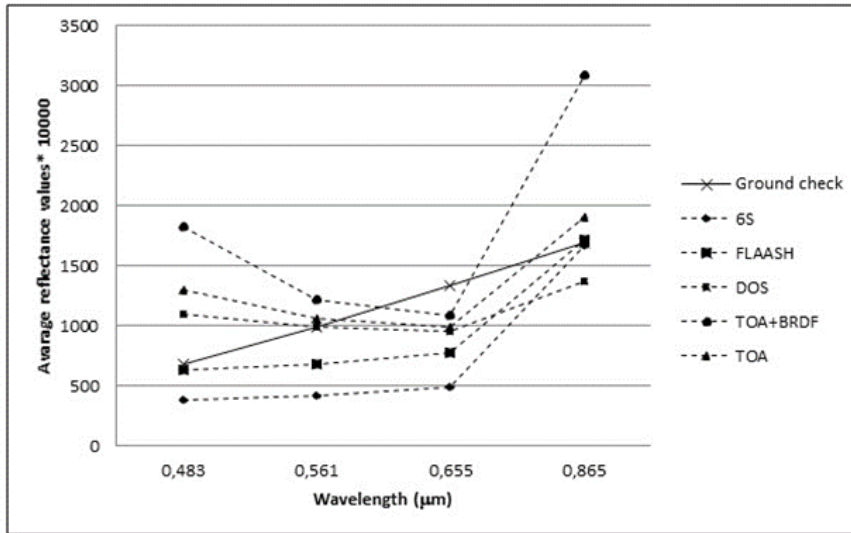


Figure 3-3: Spectral response of paddy fields location-1 in the Mundo sub-district for the TOA, TOA+BRDF, DOS, 6S, and FLAASH, compared to the field measurements

Table 3-1: Percentage of reflectance values from each spectral band of Landsat-8 for all methods compare to the field measurements at location 1 (to simplify calculations, the reflectance values are multiplied by 10.000

| Landsat-8 Spectral bands | FLAASH (%) | 6S (%) | TOA (%) | DOS (%) | TOA+BRDF (%) |
|--------------------------|------------|--------|---------|---------|--------------|
| Blue | 92 | 60 | 345 | 84 | 167 |
| Green | 68 | 61 | 258 | 93 | 124 |
| Red | 58 | 63 | 202 | 96 | 114 |
| NIR | 101 | 97 | 114 | 72 | 226 |

Table 3-2: Correlation of the reflectance values of all methods compare to the field measurements for paddy fields at location 1

| Object | Coefficient of correlation | | | | |
|--|----------------------------|--------|------|------|----------|
| | 6S | FLAASH | TOA | DOS | TOA+BRDF |
| Post-ripening phase; unvegetated soil; slightly dry and rather moist conditions (location 1) | 0.83 | 0.86 | 0.56 | 0.56 | 0.54 |

The surface reflectance value of paddy fields at location 1 derived from the FLAASH has a high correlation with field measurements with a value of 0.6. On the other hand, the reflectance value of TOA+BRDF has a low correlation with field measurements with a value of 0.54. The correlations of each atmospheric correction method are shown in Table 3-2.

The spectral response of paddy fields in the blue and green bands in the location 2 has relatively higher reflectance values for the FLAASH, DOS, TOA and TOA+BRDF methods. Among the four methods, TOA+BRDF has the highest spectral response, but that closest to the results of the field

measurements are the FLAASH, while the 6S methods has a relatively lower spectral response. The spectral response in the red band is relatively higher for the TOA, DOS and TOA+BRDF, with the highest being the TOA+BRDF, while the FLAASH and 6S tend to be lower, with the closer to the field measurement results being the FLAASH method. The spectral response in infrared bands tends to be higher for all methods, the highest being the TOA+BRDF, and the closest to the field measurements the DOS methods. In the infrared bands, the spectral response that is closest to the results of the field measurements is the FLAASH method. The spectral response of each method is shown in Figure 3-4.

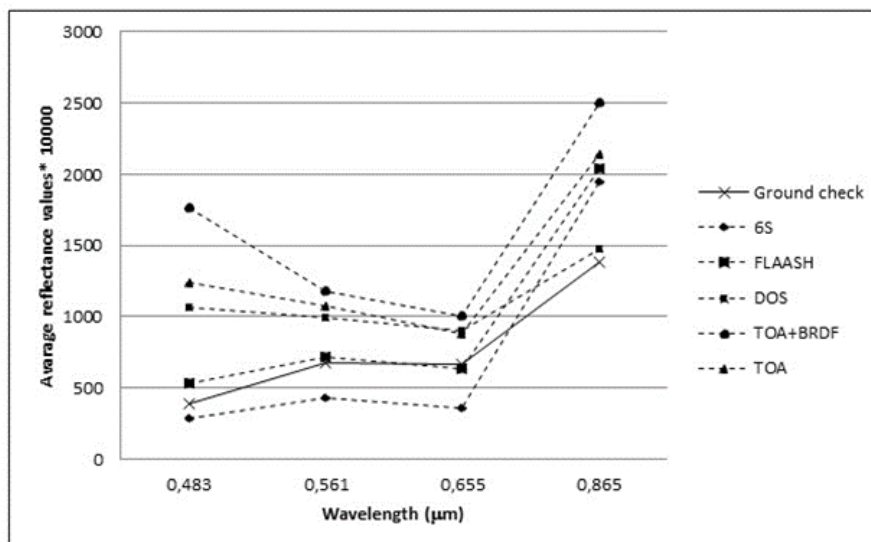


Figure 3-4: Spectral response of paddy field location 2 in the Mundo sub-district for the TOA, TOA+BRDF, DOS, 6S, FLAASH compared to the field measurements

Table 3-3: Percentage of reflectance values from each spectral band of Landsat-8 or all methods compared to the field measurements at location 2 (to simplify calculations, the reflectance values are multiplied by 10.000)

| Landsat-8 Spectral bands | FLAASH (%) | 6S (%) | TOA (%) | DOS (%) | TOA+BRDF (%) |
|--------------------------|------------|--------|---------|---------|--------------|
| Blue | 137 | 54 | 430 | 86 | 165 |
| Green | 106 | 60 | 251 | 92 | 120 |
| Red | 96 | 56 | 246 | 102 | 111 |
| NIR | 148 | 95 | 110 | 69 | 170 |

Table 3-4: Correlation of the reflectance values of each method to the field measurements for paddy fields at location 2

| Object | Coefficient of correlation | | | | |
|--|----------------------------|--------|------|------|----------|
| | 6S | FLAASH | TOA | DOS | TOA+BRDF |
| Post-ripening phase; a little grass vegetation; slightly watery soil conditions (location 2) | 0.97 | 0.97 | 0.85 | 0.85 | 0.69 |

Table 3-5: Mean values of NDVI for each method

| Object | NDVI Values | | | | | |
|--|--------------|--------|-----|-----|-----|-----------|
| | Ground Check | FLAASH | 6S | TOA | DOS | TOA+B RDF |
| Post-ripening phase; unvegetated soil; slightly dry and rather moist conditions (location 1) | 0.1 | 0.4 | 0.5 | 0.3 | 0.2 | 0.5 |
| Post-ripening phase; a little grass vegetation; slightly watery soil conditions (location 2) | 0.3 | 0.5 | 0.7 | 0.4 | 0.2 | 0.4 |

The percentages of the reflectance values of each method compared to the field measurements at location 2 are shown in Table 3-3. These also vary for each band. The highest percentage is from the TOA and TOA+BRDF as atmospheric correction has not been made. For the FLAASH, 6S and DOS method, the percentage tends to be low because for these atmosphere corrections have been made.

The reflectance values of paddy fields at location 2 which have the highest correlation to the results of the field measurements correspond to the 6S and FLAASH, at 0.97, with the lowest being for the TOA and DOS, at 0.69. The correlations of each method are shown in Table 3-4.

3.2 NDVI

The NDVI of each method has different values (Table 3-5). That of paddy fields at location 1 which is closest to the results of the field measurements is the NDVI value of the DOS, and at location 2 it is that of the TOA method.

4 CONCLUSION

Comparison of the radiometric/atmospheric correction results from the

Landsat-8 imagery with the field measurements for the object spectral responses and NDVI was made. The results show that the 6S and FLAASH have similar spectral responses to the spectral response of objects in the field, compared to the DOS, TOA and TOA+BRDF method. The NDVI value of the 6S has the same tendency as the object's NDVI value in the field.

ACKNOWLEDGEMENTS

We would like to thank Ir. Mahdi Kartasasmita MS, Ph.D., and Prof. Dr. Ir. Rr. Erna Sri Adiningsih, M.Si. for their guidance, and also the Head of the Remote Sensing Technology and Data Center, and the Head of the Programs and Facilities Division for the provision of data and infrastructure for the study.

AUTHOR CONTRIBUTIONS

The contributions of the author for each to this research paper: conceptualization and methodology: Fadila Muchsin and Supriatna; writing and preparation of original draft: Fadila Muchsin and Mulia Inda Rahayu; data processing: Fadila Muchsin, Mulia Inda Rahayu, Kuncoro Adi Pradono, and Liana Fibriawati; formal analysis: Fadila Muchsin, Supriatna, Adhi Harmoko and

Indah Prasasti; validation: Fadila Muchsin, Mulia Ina Rahayu, Kuncoro Adi Pradono, and Liana Fibriawati; writing, review and editing: Fadila Muchsin, Supriatna, Adhi Harmoko and Indah Prasasti.

REFERENCES

- Chander, G., Markham, B. L., & Helder, D. L. (2009). Summary of current radiometric calibration coefficients for Landsat MSS, TM, ETM+, and EO-1 ALI sensors. *Remote Sensing of Environment*, 113(5), 893–903. <https://doi.org/10.1016/j.rse.2009.01.007>
- Congalton, R. G. (2015). Remote Sensing and Image Interpretation. 7th Edition. *Photogrammetric Engineering & Remote Sensing* (Vol. 81). <https://doi.org/10.14358/pers.81.8.615>
- DianWang, Ma, R., Xue, K., & Loiselle, S. A. (2019). The assessment of landsat-8 OLI atmospheric correction algorithms for inland waters. *Remote Sensing*, 11(2). <https://doi.org/10.3390/rs11020169>
- ENVI. (2009). *ENVI Atmospheric Correction Module: QUAC and FLAASH user's guide*. Module Version, 44.
- Gómez, C., White, J. C., & Wulder, M. A. (2016). Optical remotely sensed time series data for land cover classification: A review. *ISPRS Journal of Photogrammetry and Remote Sensing*, 116, 55–72. <https://doi.org/10.1016/j.isprsjprs.2016.03.008>
- Hermosilla, T., Wulder, M. A., White, J. C., Coops, N. C., & Hobart, G. W. (2017). Int J Appl Earth Obs Geoinformation Updating Landsat time series of surface reflectance composites and forest change products with new observations. *Int J Appl Earth Obs Geoinformation*, 63(August), 104–111. <https://doi.org/10.1016/j.jag.2017.07.013>
- Imager, L., Barsi, J. A., Lee, K., Kvaran, G., Markham, B. L., & Pedelty, J. A. (2014). The Spectral Response of the Landsat-8 Operational Land Imager. *Remote Sensing*, 10232–10251. <https://doi.org/10.3390/rs61010232>
- Jing, Z., Wei, D., Jianxin, W., & Xuning, L. I. U. (2014). A Method to Enhance the Fog Image Based on Dark Object Subtraction, *7th International Congress on Image and Signal Processing*, 547, 2484–2487. <https://doi.org/10.4028/www.scientific.net/AMM.543-547.2484>
- Ke, Y., Im, J., Lee, J., Gong, H., & Ryu, Y. (2015). Characteristics of Landsat 8 OLI-derived NDVI by comparison with multiple satellite sensors and in-situ observations. *Remote Sensing of Environment*, 164, 298–313. <https://doi.org/10.1016/j.rse.2015.04.004>
- Kustiyo. (2017). Development of Annual Landsat 8 Composite Over Central Kalimantan, Indonesia Using Automatic Algorithm To Minimize Cloud. *International Journal of Remote Sensing and Earth Sciences (IJReSES)*, 13(1), 51. <https://doi.org/10.30536/j.ijreses.2016.v13.a2714>
- Lee, K. S., Lee, C. S., Seo, M., Choi, S., Seong, N. H., Jin, D., Han, K. S. (2020). Improvements of 6S Look-Up-Table Based Surface Reflectance Employing Minimum Curvature Surface Method. *Asia-Pacific Journal of Atmospheric Sciences*, 56(2), 235–248. <https://doi.org/10.1007/s13143-019-00164-3>
- Liang, S., Member, S., Fang, H., & Chen, M. (2001). Atmospheric Correction of Landsat ETM + Land Surface Imagery — Part I: Methods, 39(11), 2490–2498.
- Loveland, T. R., & Irons, J. R. (2016). Landsat 8: The plans, the reality, and the legacy. *Remote Sensing of Environment*, 185, 1–6. <https://doi.org/10.1016/j.rse.2016.07.033>
- Markham, B. L., & Helder, D. L. (2012). Forty-year calibrated record of earth-reflected radiance from Landsat: A review. *Remote*

- Sensing of Environment*, 122, 30–40.
<https://doi.org/10.1016/j.rse.2011.06.026>
- Moravec, D., Komárek, J., Medina, S. L. C., & Molina, I. (2021). Effect of atmospheric corrections on NDVI: Intercomparability of Landsat 8, Sentinel-2, and UAV sensors. *Remote Sensing*, 13(18), 1–15.
<https://doi.org/10.3390/rs13183550>
- Prieto-amparan, J. A., Villarreal-guerrero, F., & Martinez-salvador, M. (2018). Atmospheric and Radiometric Correction Algorithms for the Multitemporal Assessment of Grasslands Productivity. <https://doi.org/10.3390/rs10020219>
- Roy, D. P., Wulder, M. A., Loveland, T. R., C.E., W., Allen, R. G., Anderson, M. C., ... Zhu, Z. (2014). Landsat-8: Science and product vision for terrestrial global change research. *Remote Sensing of Environment*, 145, 154–172.
<https://doi.org/10.1016/j.rse.2014.02.001>
- Rumora, L., Miler, M., & Medak, D. (2020). Impact of various atmospheric corrections on sentinel-2 land cover classification accuracy using machine learning classifiers. *ISPRS International Journal of Geo-Information*, 9(4).
<https://doi.org/10.3390/ijgi9040277>
- Sterckx, S. and Wolters, E. (2019). Radiometric Top-of-Atmosphere Reflectance Consistency Assessment for Landsat 8/OLI, Sentinel-2/MSI, PROBA-V, and DEIMOS-1 over Libya-4 and RadCalNet Calibration Sites. *Remote Sensing*. 11, 2253; doi: 10.3390/rs11192253.
- Vermote, E. F., Tanré, D., Deuze, J. L., Herman, M., & Morcrette, J.-J. (1997). Second Simulation of the Satellite Signal in the Solar Spectrum, 6S: An Overview. *IEEE Transactions on Geoscience and Remote Sensing*, 35(3), 675–686.
<https://doi.org/10.1055/s-2007-963706>
- Vermote, E., Justice, C., Claverie, M., & Franch, B. (2016). Preliminary analysis of the performance of the Landsat 8/OLI land surface reflectance product. *Remote Sensing of Environment*, 185, 46–56.
<https://doi.org/10.1016/j.rse.2016.04.008>
- Wulder, M. A., White, J. C., Loveland, T. R., Woodcock, C. E., Belward, A. S., Cohen, W. B., Roy, D. P. (2016). The global Landsat archive: Status, consolidation, and direction. *Remote Sensing of Environment*, 185, 271–283.
<https://doi.org/10.1016/j.rse.2015.11.032>.

